

Rationally Designed Dynamic Superstructures Enabled by Photoaligning Cholesteric Liquid Crystals

Ling-Ling Ma, Sen-Sen Li, Wen-Song Li, Wei Ji, Bin Luo, Zhi-Gang Zheng, Zhi-Ping Cai, Vladimir Chigrinov, Yan-Qing Lu, Wei Hu,* and Lu-Jian Chen*

Self-assembled hierarchical superstructure with long-range order is of vital importance to soft materials.^[1] Liquid crystal (LC), a typical building block which allows the exquisite control of assembly behavior and resultant optical property, has received intensive attention recently.^[2] Smectic LC, a typical representative of structured materials, is characterized by well-ordered lamellar structures with the long molecular axes in a given layer being unidirectional and normal or slightly inclined to the plane of the layer.^[3] When splay deformation of the smectic LC is induced by specific physical geometry confinement,^[4] chemical surface treatment,^[5] or their combination,^[6] superstructures with various patterned macroscopic textures, such as toric focal conic domains,^[7] parabolic focal conic domains,^[8] and cylindrical oily-streak domains,^[6b,9] could be obtained. They could be used as microlens arrays,^[7a] optically selective photomasks, and so on.^[10] On the other hand, thanks to the intrinsic self-organizing ability of helical structure, hierarchical cholesteric liquid crystals (CLCs) have also attracted much attention.^[2b] Through dispersing CLCs in immiscible fluids or gels, LC microspheres^[11] and shells^[12] are obtained. These hierarchical structures could be utilized in mirrorless band-edge lasers^[11,12] and many other applications beyond displays.^[2b,13]

Compared to above CLC superstructures with sphere geometries, in-plane ones are more attractive due to great practical potentials. When CLC helical axis lies down in the plane under

a proper electric field, simple grating with parallel stripes are produced in uniformly aligned cells.^[14] Unfortunately, the defects induced by conventional mechanical rubbing technique significantly interrupt the continuity of helical axis, thus it is difficult to get orderly arranged stripes with a uniform periodicity (Figure S1, Supporting Information). That is why the so-called “fingerprint” nonuniform textures are usually reported.^[15] Moreover, the capability to manipulate the in-plane helical axes to realize more complex stripe pattern remains highly restricted. Based on the CLC in-plane aligned helical axis structure, diffraction gratings^[16] and lithography mask^[17] have been demonstrated. Moreover, the variation of the period of CLC grating^[14,18] and its rotation^[19] make it an excellent candidate for nonmechanical beam steering devices. Thus, the capability of generating high-quality CLC superstructures with ordered orientation and reliable periodicity is crucial for above applications. However, as mentioned above, the low quality and poor controllability of the self-assembled CLCs make the task very formidable. Furthermore, the present mechanical aligning technique is only suitable to produce 1D^[14,20] or 2D gratings.^[21] In case that the CLC helical axis could be rationally designed and arbitrarily controlled, new possibilities for the design of novel advanced photonic devices based on CLC superstructures will be reasonably expected. Compared to the conventional aligning technique, photoalignment is such a promising approach for high-quality LC alignment avoiding any mechanical damage, electrostatic charge, or dust contamination.^[22] It is feasible to implement this alignment for a variety of LCs,^[23] as well as LC polymers.^[24] Additionally, the technique is suitable to high-resolution multidomain alignment.^[25] Though photoalignment has been introduced to accomplish uniform planar CLCs for long,^[26] further exploring its utilization in manipulating the in-plane helical axis of CLCs may open up a door toward the creation of more fantastic hierarchical superstructures.

Here, we apply the photoalignment technique to arrange the CLC helical superstructures. Through this method, uniform and high-quality CLC gratings could easily spread all over the photoaligned region. Moreover, a dynamic photopatterning technique is adopted. The combination of the “top-down” photopatterning process with the “bottom-up” self-assembly pushes the control of CLC textures to an unprecedented level. The orientations of CLC helical axes are precisely controlled, and complex textures such as spiral stripes and wave-like gratings are demonstrated. The dynamic growing and disappearing processes of the spiral stripes, boundary confinement effect, and the relationship between designed alignments and obtained stripes are investigated. Based on several simple rules behind the CLC helical axis manipulation enabled by

L.-L. Ma, Prof. S.-S. Li, W.-S. Li, B. Luo,
Prof. Z.-P. Cai, Prof. L.-J. Chen
Department of Electronic Engineering
School of Information Science and Engineering
Xiamen University
Xiamen 361005, China
E-mail: luajianchen@xmu.edu.cn



L.-L. Ma, W. Ji, Prof. Y.-Q. Lu, Prof. W. Hu
National Laboratory of Solid State Microstructures
Collaborative Innovation Center of Advanced Microstructures
and College of Engineering and Applied Sciences
Nanjing University
Nanjing 210093, China
E-mail: huwei@nju.edu.cn
Prof. Z.-G. Zheng
Department of Physics
East China University of Science and Technology
Shanghai 200237, China

Prof. V. Chigrinov
Center for Display Research
Department of Electronic and Computer Engineering
Hong Kong University of Science and Technology
Clear Water Bay, Kowloon, Hong Kong 999077, China

DOI: 10.1002/adom.201500403

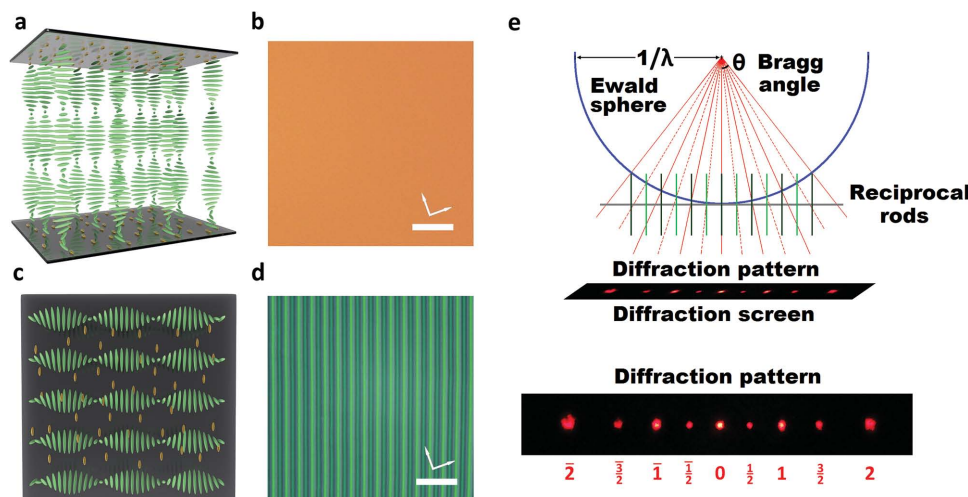


Figure 1. Schematic diagrams and corresponding images of homogeneously aligned CLCs: a,b) planar cholesteric state and c,d) electric field-induced 1D grating. The SD1 and CLC molecules are represented by yellow and green bars separately. White arrows denote the polarizer and analyzer transmission axes, respectively. The two scale bars are 20 μm . e) A geometrical simulation of the diffraction pattern based on Ewald sphere, and captured diffraction pattern with corresponding orders labeled underneath.

photoalignment, rational design, and arbitrary control of CLC fingerprint textures surpassing traditional ones can be realized. The research broadens the scientific content of self-assembly of soft materials, and may bring new superstructures with exceptional features.

To validate above design, first a uniform 1D grating is demonstrated. A polarization sensitive medium sulfonic azo dye SD1 (Figure S2, Supporting Information) is utilized as the photoalignment agent. SD1 molecules tend to reorient their absorption oscillators perpendicular to the UV light polarization and provide an azimuthal anchoring energy over 10^{-4} J m^{-2} , which is comparable with that of rubbed polyimide films.^[27] Both alignment layers on the substrates need to be exposed simultaneously by a linearly polarized UV light to form a homogeneous alignment. In this condition, as shown in **Figure 1a**, the CLC molecules adjacent to the alignment layers follow the induced orientation of SD1, and the internal molecules self-assemble into a helical structure spontaneously with the helical axis normal to the substrates. Herein, the cell gap d is $4.8 \pm 0.2 \mu\text{m}$ and the equilibrium pitch p of CLC is $\approx 3.0 \mu\text{m}$, resulting $d/p = 1.6$. The ratio is slightly larger than 1.5, thus a helical structure with one and a half pitches is arranged in the cell due to the surface anchoring. Corresponding planar cholesteric texture is observed under a polarized optical microscope (POM). A uniform reddish color is shown in **Figure 1b**, which indicates a good alignment quality. When a proper electric field is applied across the cell, the helical axis reorients to form an in-plane orientation perpendicular to the original alignment, as depicted in the top view scheme (**Figure 1c**). This phenomenon is because of the dielectric anisotropy induced reorientation of CLCs and the twisted power of chiral dopant caused maintenance of helical structure.^[28] The exact direction of helical axis is determined by both the d/p ratio and the alignment condition.^[18,29] In our work, when AC voltage (2.4 V, $f = 1 \text{ kHz}$) is applied, a grating is generated due to the periodic variation of refractive index along the helical axis (**Figure 1d**).

As mentioned previously, the introduction of noncontact photoalignment is expected to drastically improve the quality and uniformity of the CLC diffraction gratings. In our experiment, uniform green stripes as presented in **Figure 1d** are observed in the whole cell. To further inspect the performance of CLC grating, an He–Ne laser (633 nm) with polarization perpendicular to the grating vector is normally incident to the cell, and the resultant diffraction pattern (bottom image in **Figure 1e**) is captured by a digital camera. According to the parameters of ± 1 st orders, a grating period Λ of $1.5 \mu\text{m}$ is calculated, which is consistent with the period of refractive index change ($p/2$). Besides integer orders, half-integer ones could also be observed, which is associated with the secondary grating structure with doubled period (i.e., $\Lambda' = p$) generated in the same cell.^[30] The distance between two adjacent diffraction spots l increases as the diffraction order n increases. The reciprocal space and Ewald sphere in crystallography is applied to explain the obtained diffraction pattern (**Figure 1e**).^[31] In a reciprocal space, the CLC grating stripes are turned into a set of rods parallel to each other named reciprocal rods. The diffraction pattern is the objection of the intersection points of the reciprocal rods and the Ewald sphere to the diffraction screen. In this case, the wavelength of He–Ne laser is 633 nm, giving the Ewald sphere a radius of $1/\lambda = 1.58 \mu\text{m}^{-1}$. Because the grating period Λ is $1.5 \mu\text{m}$, the distance of adjacent reciprocal rods is $0.67 \mu\text{m}^{-1}$. From the geometric relationship, we got diffraction pattern with certain diffraction angles θ_n . The ratio of l_{n+1} to l_n is $2\cos\theta_n/\cos\theta_{n+1} - 1$. Since $\theta_n < \theta_{n+1} < 90^\circ$, the ratio is larger than 1, leading to significantly increasing of l . The positions of both integer and half-integer spots given on the diffraction screen are consistent with the experimental results. In spite of a slight beam extension in higher orders, the results in our work are much better than those achieved via traditional aligning techniques. Besides, the diffraction patterns are the same in different cell regions, which indicates that the photoalignment technique is suitable for the preparation of large area and defect-free CLC gratings.

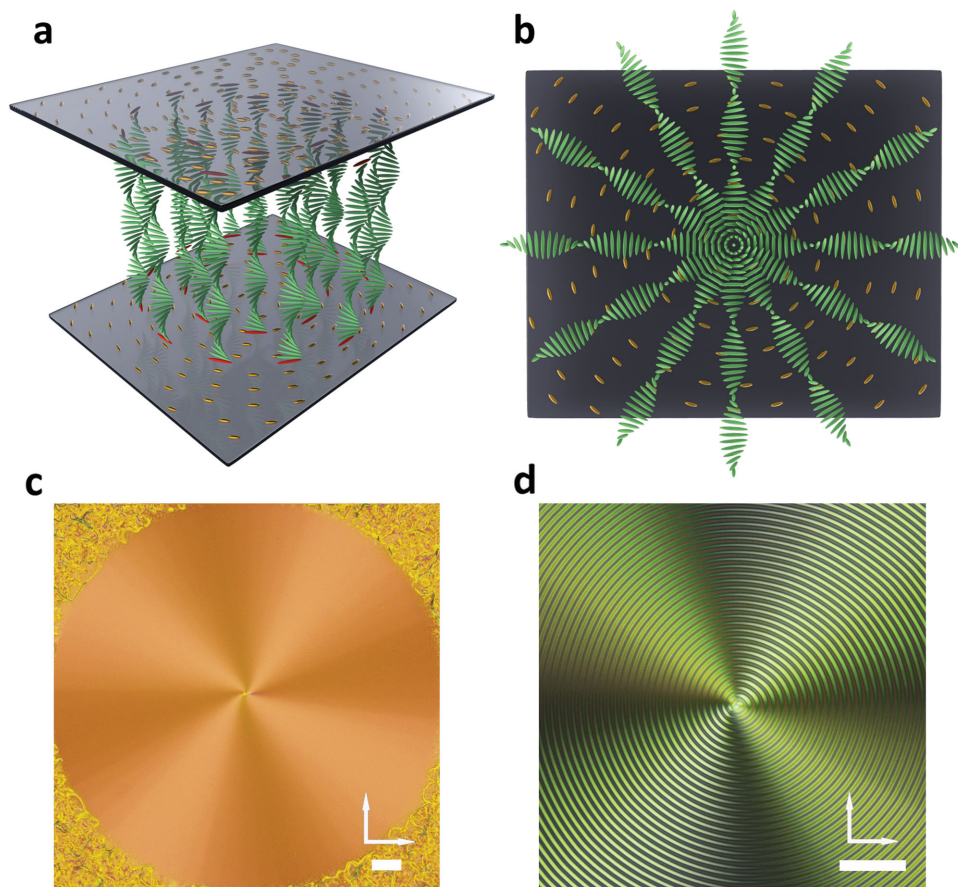


Figure 2. a,b) Schematic diagrams and c,d) corresponding images of circularly aligned CLCs in planar cholesteric state and electric field-induced spiral stripe state. The SD1 and CLC molecules are represented by yellow and green bars separately. The CLC directors adjacent to the substrates are marked in red. White arrows denote the polarizer and analyzer transmission axes, respectively. The two scale bars are 50 μm .

To further explore the capability of CLC helical axis manipulation, an azimuthally aligned cell is fabricated. The specific alignment is accomplished via photoreorientation of SD1 on a dynamic microlithography system.^[25] After the CLCs infiltrated, the orientations of SD1 and director distribution of CLCs are schematically illustrated in **Figure 2a**. Similar to the homogeneous case, all the helical axes stand normal to the cell. The CLC molecules adjacent to the alignment layers are fixed parallel to the local orientation of SD1, causing a different phase retardation to a linearly polarized light. The generated planar texture reveals a reddish birefringence color as presented in **Figure 2c**. After the voltage is applied, the helical axes realign radially, i.e., perpendicular to SD1 orientations (**Figure 2b**). Accordingly, “concentric” rings of dark-bright alternations are formed due to the periodic refractive index modulation. **Figure 2d** exhibits a spiral stripe pattern fulfilling the entire photoaligned region. It is worth mentioning that the Maltese crosses, where the aligning direction is either parallel or perpendicular to the incident polarization, is clearly observed in both **Figure 2c,d**.

The growing process of the CLC spiral stripes is also investigated. When a voltage of 2.0 V is applied, golden radialized stripes emerge in a manner similar to the development of a photographic image, therefore it is called developable

modulation (DM).^[32] The DM type texture is composed of stable but nonuniform stripes at the relatively low voltage. When the voltage increases to 2.4 V, an Archimedean spiral, the so-called growing-modulation (GM) type,^[32] grows clockwise from the central singularity point. As presented in **Figure 3a**, the stripe winds azimuthally and expands its territory via gradually replacing the DM texture. Compared to the large quantity of uncontrollable defects in DM type, only few defects could be observed here. The dislocation structures with Burgers vector equals to $p/2$ play important roles in the growing of GM-type texture.^[16] They help to readjust the whole texture to achieve an equilibrium, making the spiral more rounded. **Figure 3b** shows the concentric diffraction pattern of the CLC spiral stripes, with coincident symmetry. Two splits are observed in each circle, as no periodic refractive index variation occurs for a horizontal incident polarization.

Further increasing the voltage, the well-formed spiral stripes will be unwound. As shown in **Figure 3c**, After the voltage increases to 4.0 V, the CLC spiral stripes shorten from both terminals at the beginning. Subsequently, several dislocations, which play key roles in the annihilation of the spiral stripe,^[33] appear and the stripes begin loosening up from a tight state to reach a no-stripe-left state. When a voltage of 10.0 V is applied, the Maltese cross can still be distinguished due to the residual

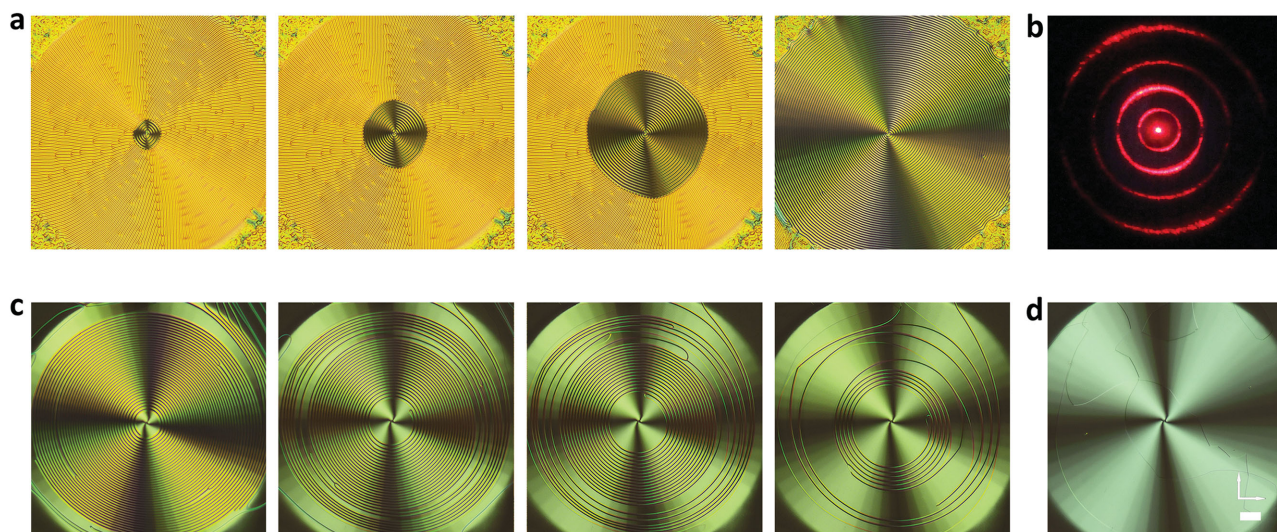


Figure 3. a) The changing process from DM type to GM type when a voltage of 2.4 V is applied. b) The diffraction pattern of the CLC spiral stripes. c) The disappearing of CLC spiral stripes when a voltage of 4.0 V is applied. d) A no-stripe-left state when a voltage of 10.0 V is applied. White arrows denote the polarizer and analyzer transmission axes, respectively. The scale bar is 50 μm .

phase retardation as shown in Figure 3d. When the voltage is high enough to align the LC molecules vertically, a uniform dark state will be obtained. After the voltage is removed, the disappearing process of CLC spiral stripes is also recorded and corresponding results are presented in Figure S3 (Supporting Information).

To find out general rules behind the CLC helical axis manipulation enabled by photoalignment, we systematically study the relationship between the designed alignments and the directions of obtained stripes in two contiguous domains. The

included angles α between two alignment directions of the three samples are 80° , 60° , and 95° , respectively (Figure 4a–c). Disclination lines are observed at the domain boundaries, where the LC director suffers a sudden change and causes discontinuity. Such disclination line occurs when $\alpha < 95^\circ$. It is worth mentioning that if one alignment angle with respect to the disclination line is smaller than 20° , the generated stripes will deviate from the original alignment and follow the direction of the disclination line (Figure 4a). This boundary-confinement effect, which facilitates the energy dissipation, could also

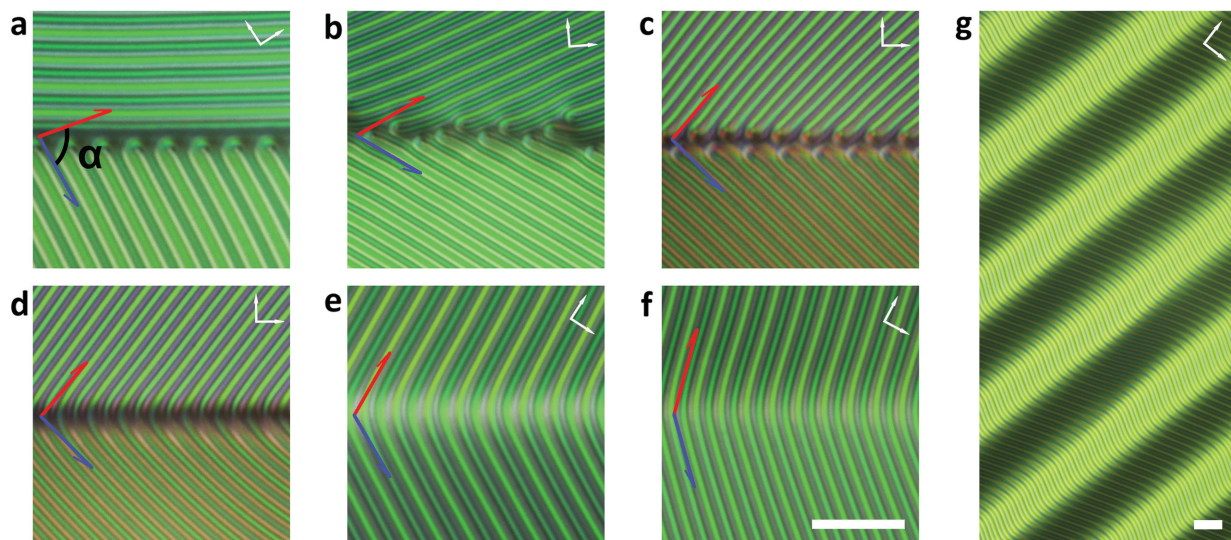


Figure 4. Multidomain CLC stripes. The aligning directions in the top and bottom domains are indicated as red and blue arrows, respectively, and corresponding alignment angles are: a) 20° , -60° ; b) 30° , -30° ; c,d) 50° , -45° ; e) 60° , -60° ; and f) 75° , -75° . The included angle between two alignment directions is denoted as α . g) A wave-like CLC grating. White arrows denote the polarizer and analyzer transmission axes, respectively. The scale bars are 20 μm .

be utilized to guide the orientation of helical axis and affect the final appearance of the textures (Figure S4, Supporting Information). It is notable that 95° is a critical angle between continuous and discontinuous stripes. In our experiment, both states are observed in the range of $95 \pm 5^\circ$ as shown in Figure 4c,d. When further increasing the included angle, only continuous CLC stripes appear, as exhibited in Figure 4e,f. Therefore, in the range of 100° – 180° , the helical axis could be arbitrarily controlled by photoalignment. With these general rules, we can rationally design the alignment and precisely orient the CLC helical axis, making more complex textures achievable. As an example, a wave-like continuous grating is demonstrated through a spatially variant alignment (Figure 4g).

Based on the photoalignment technique, a simple and straightforward way to control the orientation of CLC helical axis is presented. By this means, large-scale and defect-free CLC gratings are prepared. With the aid of a dynamic photopatterning process, more complex CLC superstructures and resultant periodic ribbon-shaped textures are generated. The self-assembled systems here are dynamic ones, which could be readily produced or erased due to the reversible and noncovalent interactions among the CLC molecules. Besides, thanks to the intrinsic feature of CLCs, a distinctive capability of generating various featured sizes ranging from the micrometer to the submicrometer scale is provided. The proposed technique shows the merits of high quality, excellent flexibility, easy fabrication, cost-efficient, and suit to mass production. It drastically enhances the capability for the creation of hierarchical superstructure with long-range order, and might trigger the exploration toward novel helical superstructures that may bring brand new opportunities to advanced photonic devices and lithography processes.

Experimental Section

Materials: The CLC mixture was composed of nematic E7 (Merck) and chiral agent S811 (Merck). The concentration of S811 in the CLC mixture was ≈ 3 wt%, with a helical twisted power value of $11.3 \mu\text{m}^{-1}$ at room temperature. In the photoaligning process, 0.3% solution of sulfonic azo dye SD1 (Dai-Nippon Ink and Chemicals, Japan) in dimethylformamide (DMF) was used.

Cell Preparations: The two indium tin oxide (ITO)-coated glass substrates were ultrasonic bathed, UV–ozone cleaned, and then spin-coated with SD1. Then the substrates were assembled together and separated by UV glue doped with 7 wt% $5 \mu\text{m}$ spacers. Afterward, the empty cell was placed at the image plane of the digital micromirror device (DMD) based microlithography system to record the designed aligning pattern. After that, the CLC mixture was heated to 65°C and filled into the cell.

Photoalignment Process: A DMD based microlithography system^[25a] was used to carry out the photoalignment process. A multistep partly overlapping exposure process^[25c] was employed. The continuously varied SD1 orientations were accomplished by exposing specific region with given polarization. After a total exposure dose of $\approx 5 \text{ J cm}^{-2}$, the desired orientation of SD1 would be achieved.

Characterizations: The CLC textures were observed under a cross-polarized optical microscope (Nikon 50i, Japan). The diffraction patterns were captured by a digital camera (Canon EOS, 600D).

Supporting Information

Supporting Information is available from the Wiley Online Library or from the author.

Acknowledgements

This work was sponsored by the National Natural Science Foundation of China (Nos. 61490714, 61575093, 61435008, and 11304151), the Fundamental Research Funds for the Central Universities (No. 20720140518), the Ph.D. Programs Foundation of the Ministry of Education of China (No. 20120091120020), and the Open Foundation Project of National Laboratory of Solid State Microstructures (M28007). The authors thank Hao Qian and Kang-Jun Lin for their assistance in drawing the schemes.

Received: July 22, 2015

Revised: August 17, 2015

Published online: September 7, 2015

- [1] a) G. M. Whitesides, B. Grzybowski, *Science* **2002**, *295*, 2418; b) J. V. Barth, G. Costantini, K. Kern, *Nature* **2005**, *437*, 671.
- [2] a) Y. H. Kim, D. K. Yoon, H. S. Jeong, O. D. Lavrentovich, H. T. Jung, *Adv. Funct. Mater.* **2011**, *21*, 610; b) H. K. Bisoyi, Q. Li, *Acc. Chem. Res.* **2014**, *47*, 3184.
- [3] J. Prost, *The Physics of Liquid Crystals*, Oxford University Press, New York, USA **1995**.
- [4] a) D. K. Yoon, M. C. Choi, Y. H. Kim, M. W. Kim, O. D. Lavrentovich, H. T. Jung, *Nat. Mater.* **2007**, *6*, 866; b) A. Honglawan, D. A. Beller, M. Cavallaro, R. D. Kamien, K. J. Stebe, S. Yang, *Proc. Natl. Acad. Sci. USA* **2013**, *110*, 34; c) A. Honglawan, D. A. Beller, M. Cavallaro, R. D. Kamien, K. J. Stebe, S. Yang, *Adv. Mater.* **2011**, *23*, 5519.
- [5] Y. H. Kim, D. K. Yoon, H. S. Jeong, J. H. Kim, E. K. Yoon, H. T. Jung, *Adv. Funct. Mater.* **2009**, *19*, 3008.
- [6] a) J. M. Ok, Y. H. Kim, H. S. Jeong, H. W. Yoo, J. H. Kim, M. Srinivasarao, H. T. Jung, *Soft Matter* **2013**, *9*, 10135; b) D. Coursault, J. Grand, B. Zappone, H. Ayeb, G. Levi, N. Felidj, E. Lacaze, *Adv. Mater.* **2012**, *24*, 1461.
- [7] a) Y. H. Kim, H. S. Jeong, J. H. Kim, E. K. Yoon, D. K. Yoon, H. T. Jung, *J. Mater. Chem.* **2010**, *20*, 6557; b) T. Ohzono, Y. Takenaka, J. I. Fukuda, *Soft Matter* **2012**, *8*, 6438.
- [8] a) C. Wolf, A. M. Menzel, *J. Phys. Chem. B* **2008**, *112*, 5007; b) B. I. Senyuk, I. I. Smalyukh, O. D. Lavrentovich, *Phys. Rev. E* **2006**, *74*, 011712.
- [9] a) J. P. Michel, E. Lacaze, M. Alba, M. de Boissieu, M. Gailhanou, M. Goldmann, *Phys. Rev. E* **2004**, *70*, 011709; b) B. Zappone, E. Lacaze, *Phys. Rev. E* **2008**, *78*, 061704.
- [10] Y. H. Kim, J. O. Lee, H. S. Jeong, J. H. Kim, E. K. Yoon, D. K. Yoon, J. B. Yoon, H. T. Jung, *Adv. Mater.* **2010**, *22*, 2416.
- [11] a) Z. G. Zheng, B. W. Liu, L. Zhou, W. Wang, W. Hu, D. Shen, *J. Mater. Chem. C* **2015**, *3*, 2462; b) M. Humar, I. Mušević, *Opt. Express* **2010**, *18*, 26995; c) G. Cipparrone, A. Mazzulla, A. Pane, R. J. Hernandez, R. Bartolino, *Adv. Mater.* **2011**, *23*, 5773.
- [12] a) L. J. Chen, Y. N. Li, J. Fan, H. K. Bisoyi, D. A. Weitz, Q. Li, *Adv. Opt. Mater.* **2014**, *2*, 845; b) Y. Uchida, Y. Takanishi, J. Yamamoto, *Adv. Mater.* **2013**, *25*, 3234.
- [13] W. Hu, H. Zhao, L. Song, Z. Yang, H. Cao, Z. Cheng, Q. Liu, H. Yang, *Adv. Mater.* **2010**, *22*, 468.
- [14] H. C. Jau, Y. Li, C. C. Li, C. W. Chen, C. T. Wang, H. K. Bisoyi, T. H. Lin, T. J. Bunning, Q. Li, *Adv. Opt. Mater.* **2015**, *3*, 166.
- [15] J. Baudry, S. Pirkel, P. Oswald, *Phys. Rev. E* **1998**, *57*, 3038.
- [16] D. Subacius, P. J. Bos, O. D. Lavrentovich, *Appl. Phys. Lett.* **1997**, *71*, 1350.
- [17] H. S. Jeong, Y. H. Kim, J. S. Lee, J. H. Kim, M. Srinivasarao, H. T. Jung, *Adv. Mater.* **2012**, *24*, 381.
- [18] A. Y. G. Fuh, C. H. Lin, C. Y. Huang, *Jpn. J. Appl. Phys.* **2002**, *41*, 211.
- [19] a) C.-H. Lin, R.-H. Chiang, S.-H. Liu, C.-T. Kuo, C.-Y. Huang, *Opt. Express* **2012**, *20*, 26837; b) A. Ryabchun, A. Bobrovsky, J. Stumpe, V. Shibaev, *Adv. Opt. Mater.* **2015**, DOI: 10.1002/adom.201500159;

- c) A. Ryabchun, A. Bobrovsky, J. Stumpe, V. Shibaev, *Adv. Opt. Mater.* **2015**, DOI: 10.1002/adom.201500293.
- [20] D. Subacius, S. V. Shiyankovskii, P. Bos, O. D. Lavrentovich, *Appl. Phys. Lett.* **1997**, *71*, 3323.
- [21] B. I. Senyuk, I. I. Smalyukh, O. D. Lavrentovich, *Opt. Lett.* **2005**, *30*, 349.
- [22] a) O. Yaroshchuk, Y. Reznikov, *J. Mater. Chem.* **2012**, *22*, 286; b) V. G. Chigrinov, V. M. Kozenkov, H. S. Kwok, *Photoalignment of Liquid Crystalline Materials: Physics and Applications*, Wiley, West Sussex, England, UK **2008**.
- [23] a) X. W. Lin, W. Hu, X. K. Hu, X. Liang, Y. Chen, H. Q. Cui, G. Zhu, J. N. Li, V. G. Chigrinov, Y. Q. Lu, *Opt. Lett.* **2012**, *37*, 3627; b) W. Hu, A. Kumar Srivastava, X. W. Lin, X. Liang, Z. J. Wu, J. T. Sun, G. Zhu, V. G. Chigrinov, Y. Q. Lu, *Appl. Phys. Lett.* **2012**, *100*, 111116; c) A. K. Srivastava, W. Hu, V. G. Chigrinov, A. D. Kiselev, Y. Q. Lu, *Appl. Phys. Lett.* **2012**, *101*, 031112.
- [24] a) M. Schadt, H. Seiberle, A. Schuster, S. M. Kelly, *Jpn. J. Appl. Phys.* **1995**, *34*, L764; b) M. Schadt, K. Schmitt, V. Kozinkov, V. Chigrinov, *Jpn. J. Appl. Phys.* **1992**, *31*, 2155.
- [25] a) H. Wu, W. Hu, H. C. Hu, X. W. Lin, G. Zhu, J. W. Choi, V. G. Chigrinov, Y. Q. Lu, *Opt. Express* **2012**, *20*, 16684; b) B. Y. Wei, W. Hu, Y. Ming, F. Xu, S. Rubin, J. G. Wang, V. G. Chigrinov, Y. Q. Lu, *Adv. Mater.* **2014**, *26*, 1590; c) P. Chen, B. Y. Wei, W. Ji, S. J. Ge, W. Hu, F. Xu, V. G. Chigrinov, Y. Q. Lu, *Photonics Res.* **2015**, *3*, 133.
- [26] M. Schadt, K. Schmitt, presented at *SID Proc. Int. Display Research Conf.*, Boston, December **1997**.
- [27] H. Akiyama, T. Kawara, H. Takada, H. Takatsu, V. Chigrinov, E. Prudnikova, V. Kozenkov, H. Kwok, *Liq. Cryst.* **2002**, *29*, 1321.
- [28] S. T. Wu, D. K. Yang, *Fundamentals of Liquid Crystal Devices*, Wiley, West Sussex, England, UK **2014**.
- [29] a) J.-J. Wu, Y.-S. Wu, F.-C. Chen, S.-H. Chen, *Jpn. J. Appl. Phys.* **2002**, *41*, L1318; b) H.-C. Jau, T.-H. Lin, Y.-Y. Chen, C.-W. Chen, J.-H. Liu, A. Y. G. Fuh, *Appl. Phys. Lett.* **2012**, *100*, 131909.
- [30] S. W. Kang, S. Sprunt, L. C. Chien, *Appl. Phys. Lett.* **2000**, *76*, 3516.
- [31] D. B. Williams, C. B. Carter, *The Transmission Electron Microscope*, Springer, New York, USA **1996**.
- [32] O. D. Lavrentovich, S. V. Shiyankovskii, D. Voloschenko, *Proc. SPIE* **1999**, *3787*, 149.
- [33] M. Kawachi, O. Kogure, *Jpn. J. Appl. Phys.* **1977**, *16*, 7.